Piezo-optical coefficients of ZnSe and ZnTe above the fundamental gap

D. Rönnow, M. Cardona, and L. F. Lastras-Martínez
Max-Planck-Institut für Festkörperforschung, Heisenbergstrasse 1, 70569 Stuttgart, Germany
(Received 19 August 1998)

The piezo-optical coefficients $P_{11}-P_{12}$ and P_{44} have been measured for ZnSe and ZnTe above the fundamental gap (in the energy ranges 2.6−5.5 eV and 2.0−5.5 eV, respectively) by using reflectance difference spectroscopy. The measured spectra of $P_{11}-P_{12}$ and P_{44} show good Kramers-Kronig consistency between their real and imaginary parts. Values for the deformation potentials D_1^5, D_3^3, and D_3^5 for the E_1 and $E_1+\Delta_1$ transitions were estimated by fitting the spectral dependence of $P_{11}-P_{12}$ and P_{44} to analytical line shapes based on a one-electron approximation. [S0163-1829(99)08707-X]

I. INTRODUCTION

Wide band-gap semiconductors have been intensely studied during the last decade because of their potential use in, e.g., short-wavelength lasers and electronics for high temperatures.[1] The electronic and optical properties of epitaxial layers can be changed by built-in stress, a feature that can be used to tailor these properties.[2] The measurement of the piezo-optical properties of semiconductors is a powerful technique to obtain information about the electronic structure and the way it changes with stress or strain.[3,4] Hence, the piezo-optical properties of Si (Ref. 5) and Ge (Ref. 6) as well as GaAs (Ref. 9) and InP (Refs. 10–12) have been extensively investigated, not only in the transparent region below the fundamental gap E_0 but also in the absorbing region above E_0.

A review of the optical properties of cubic, unstressed ZnSe and ZnTe was given by Ward.[13] In the last years several reports of ellipsometric measurements of the optical properties of ZnSe (Refs. 14–17) and ZnTe (Refs. 18–20) above E_0 have appeared. The piezo-optical coefficients of ZnSe *below* E_0 have been measured by piezo-birefringence techniques at room temperature[21,22] as well as at low temperature[23] and by an acousto-optical technique at room temperature.[24] There are also data for the piezo-optical coefficients below E_0 derived from Brillouin scattering[25] and piezo-optical coefficients measured on polycrystalline samples.[26,27] The change in refractive index with uniaxial stress has also been measured around E_0 and $E_0+\Delta_0$ at room and low temperatures.[28,29]

Deformation potentials of the E_0 transition in ZnSe have been determined by fitting experimental data for the piezo-optical coefficients to analytical expressions based on a one-electron approximation,[24,25,21] by performing photoluminescence measurements on strained epilayers,[30] and by two-photon spectroscopy under uniaxial stress.[31] The change in E_0 with hydrostatic stress has also been used to determine the corresponding deformation potential.[32,29] Several authors have also determined E_0 deformation potentials of ZnSe epilayers.[28,33–35] The E_0 transition of ZnSe has been studied using band-structure theory and the corresponding deformation potentials have been calculated.[32,36–38]

ZnSe exhibits also stress-induced optical activity[39,40] and has been found to be naturally birefringent below E_0 as a result of spatial dispersion.[41–43] These two effects are several orders of magnitude smaller than the stress-induced birefringence and we neglect them in the present investigation [they are proportional to (a_0/λ) and $(a_0/\lambda)^2$, respectively, where a_0 is the lattice constant and λ the wavelength of the light].[44]

For ZnTe the piezo-optical coefficients have been measured *below* E_0 by means of piezo-birefringence[21] and Brillouin scattering.[45,46] The hydrostatic deformation potential of the E_0 transition has also been determined.[47]

In this paper, we report measurements of the piezo-optical coefficients $P_{11}-P_{12}$ and P_{44} of ZnSe and ZnTe *above* E_0. Ellipsometry and piezo-birefringence have been used previously to determine the piezo-optical coefficients of elemental and III-V semiconductors above E_0. ZnSe and ZnTe are more brittle than these materials. We therefore had to use reflectance difference spectroscopy (RDS) to determine their piezo-optical coefficients. RDS is sometimes referred to as reflectance anisotropy spectroscopy (RAS). Details of the experiments are given elsewhere.[48]

Theoretical studies of piezo-optical properties of semiconductors have been concerned with elemental and III-V compounds. Tight-binding calculations have been used to elucidate the piezo-optical coefficients of Si,[49] Ge,[50] and InP (Ref. 10) whereas pseudopotential calculations have been used for Si,[5,51] Ge,[6] and GaAs.[9] To the best of our knowledge no calculations of the piezo-optical coefficients of II-VI compounds have been reported. *Ab initio* calculations of the deformations potentials of the E_1 transitions of Ge, GaAs, InP, ZnSe, and ZnTe will be presented elsewhere.[7]

The paper is organized as follows: The experiments are briefly described in Sec. II. In Sec. III, the pseudodielectric functions $\varepsilon(\omega)$ of ZnSe and ZnTe as obtained from ellipsometry are presented. Standard analytical line shapes are used to represent the E_1 and $E_1+\Delta_1$ transitions and determine line-shape parameters. The measured piezo-optical coefficients are presented in Sec. IV. In Sec. V, deformation potentials of the E_1 and $E_1+\Delta_1$ transitions are determined from those piezo-optical coefficients, using line-shape parameters from Sec. III. Section VI contains a discussion of the results and Sec. VII the conclusions.

II. EXPERIMENT

We used undoped ZnSe and ZnTe single crystals. The samples were cut in $18\times2.8\times1.8$-mm^3 pieces with the long-

est side parallel to the [001] and [111] crystal directions, respectively, and oriented using Laue x-ray diffraction. For these samples, $\varepsilon(\omega)$ was determined by means of rotating analyzer ellipsometry. RDS (Ref. 8) was used to determine the shear piezo-optical coefficients. In RDS the difference in the complex Fresnel coefficients $\Delta r/r=(\varepsilon_a-\varepsilon_b)/[\sqrt{\varepsilon}(\varepsilon-1)]$ $[\Delta r=r_a-r_b;\ r=(r_a+r_b)/2]$ between two orthogonal axes a and b is measured. Compressive uniaxial stress was applied along the [001] and [111] crystal directions. The applied stress gives rise to a difference in $\varepsilon(\omega)$ between the components parallel and perpendicular to the stress. This stress-induced anisotropy was measured with RDS. Stresses up to 0.05 GPa were used. [As a comparison, for GaAs (Ref. 9) and InP (Ref. 10) stresses up to 0.7 GPa were used.] The measurements were performed on (211) surfaces, in air and at room temperature. The use of RDS for determining piezo-optical coefficients and the experimental details have been discussed elsewhere.[48]

III. DIELECTRIC FUNCTION

When determining the deformation potentials of the E_1 and $E_1+\Delta_1$ transitions from the piezo-optical coefficients one needs to know the line-shape parameters of $\varepsilon(\omega)$ at these transitions. We use the standard analytical line shape[52]

$$\varepsilon(\omega)=C-Ae^{i\phi}(\hbar\omega-E_i+i\Gamma)^n, \tag{1}$$

where A represents the strength of the critical point, E_i the transition energy, Γ the broadening, ϕ an excitonic phase angle, and $\hbar\omega$ the photon energy. For a one-dimensional critical point $n=-1/2$, for a two-dimensional critical point $n=0$ [i.e., $\varepsilon(\omega)\sim\ln(\hbar\omega-E+i\Gamma)$], and for a three-dimensional critical point $n=1/2$. Discrete excitons correspond to $n=-1$.

When determining the line-shape parameters from experimental data we analyze the second derivative with respect to energy, i.e., we use the line shapes

$$\frac{d^2\varepsilon(\omega)}{d(\hbar\omega)^2}=\begin{cases}-n(n-1)Ae^{i\phi}(\hbar\omega-E_i+i\Gamma)^{n-2}, & n\neq 0\\ Ae^{i\phi}(\hbar\omega-E_i+i\Gamma)^{-2}, & n=0.\end{cases} \tag{2}$$

Equations (1) and (2) have been derived using a one-electron approximation with parabolic bands and matrix elements independent of **k**. Excitonic effects are taken into account only through the phase angle ϕ. It should be underlined that Eqs. (1) and (2) are only reliable for difference or differential spectra.[52]

A. $\varepsilon(\omega)$ of ZnSe

The pseudodielectric function $\varepsilon(\omega)$ of ZnSe as measured by ellipsometry at room temperature is shown in Fig. 1. Ellipsometric measurements are known to be sensitive to the presence of oxide layers on the sample. Hence, the data were corrected using a three-phase model (material-overlayer-air).[53] The optical properties of the native oxide of ZnSe are not known. We therefore used data for the native oxide for GaAs,[54] which has been found to model remarkably well overlayer effects on ZnSe.[17] For the sample material we used the data reported by Kim and Sivananthan.[17]

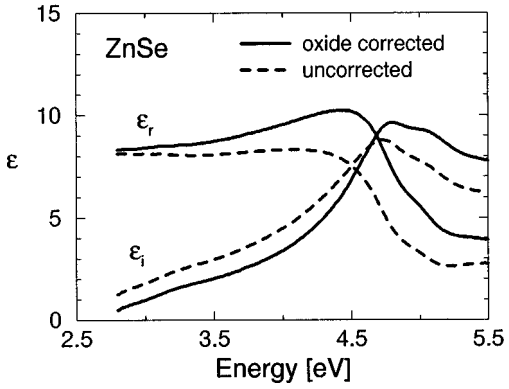

FIG. 1. Real (ε_r) and imaginary (ε_i) parts of the pseudodielectric function of unstressed ZnSe as measured by ellipsometry at room temperature. Data corrected and uncorrected for the presence of an oxide overlayer are given.

The overlayer thickness was then found to be 26 Å. Figure 1 displays data corrected as well as uncorrected for a surface overlayer.

In Fig. 2 the second derivatives with respect to energy of Re$[\varepsilon(\omega)]$ and Im$[\varepsilon(\omega)]$, corrected for overlayer effects, are given in the vicinity of the E_1 and $E_1+\Delta_1$ transitions. We use excitonic line shapes, i.e., $n=-1$ in Eq. (2), to fit these second derivatives. Such line shapes have previously been found to best reproduce the experimental spectra of the E_1 and $E_1+\Delta_1$ transitions in ZnSe.[15] The real and imaginary parts were fitted simultaneously. The fitted curves are given in Fig. 2 and the fitted line-shape parameters in Table I. For comparison, we also used a two-dimensional line shape, i.e., $n=0$ in Eq. (2), to fit the second derivatives of $\varepsilon(\omega)$. The fitting parameters are given in Table I.

B. $\varepsilon(\omega)$ of ZnTe

In Fig. 3 $\varepsilon(\omega)$ of ZnTe, as measured by ellipsometry, is displayed. Again, we used a three-phase model and data obtained by ellipsometry for the ZnTe sample[20] and the native oxide of GaAs (Ref. 54) to correct for the surface overlayer.

The second derivatives of Re$[\varepsilon(\omega)]$ and Im$[\varepsilon(\omega)]$ (corrected for a surface overlayer) with respect to energy are

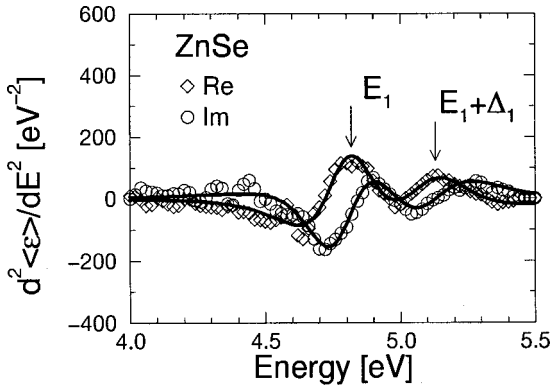

FIG. 2. Second derivative of the pseudodielectric function of ZnSe, as corrected for a surface overlayer, shown in Fig. 1 in the vicinity of the E_1 and $E_1+\Delta_1$ transitions. The solid lines represent fitted values obtained with the excitonic line shape of Eq. (2). The corresponding fitted parameters are given in Table I.

TABLE I. Critical point parameters of the E_1 and $E_1+\Delta_1$ transitions in ZnSe and ZnTe, obtained by fitting Eq. (2) to the ellipsometric data shown in Figs. 2 and 4, respectively. Rows 1–5 are parameters for two-dimensional critical points ($n=0$) and rows 7–11 correspond to exciton line shapes ($n=-1$). Row 6 contain theoretical values for the strengths of a two-dimensional critical point, calculated with Eqs. (A1a) and (A1b). Theoretical values for the strengths calculated using an excitonic model, Eqs. (A2a) and (A2b), are given in row 12.

	ZnSe E_1	ZnSe $E_1+\Delta_1$	ZnTe E_1	ZnTe $E_1+\Delta_1$
n	0	0	0	0
E (eV)	4.75	5.07	3.60	4.18
Γ (eV)	0.15	0.12	0.14	0.18
ϕ (deg)	89	89	136	136
A	5.01	1.62	5.26	4.07
A_{th}	1.6	1.5	2.1	1.6
n	−1	−1	−1	−1
E (eV)	4.79	5.10	3.60	4.18
Γ (eV)	0.23	0.30	0.21	0.26
ϕ (deg)	58	58	17	17
A (eV)	1.09	1.24	1.62	1.50
A_{th} (eV)	0.45	0.40	0.26	0.22

given in Fig. 4. For ZnTe in order to fit our data we use the line shapes of a two-dimensional critical point [$n=0$ in Eq. (2)], which have been found to give the best agreement with experiment.[18] Real and imaginary parts were fitted simultaneously. The fitted curves are shown in Fig. 4 and the obtained line-shape parameters are given in Table I. An excitonic line shape [$n=-1$ in Eq. (2)] was also used to fit the second derivatives; the obtained line-shape parameters are given in Table I.

IV. PIEZO-OPTICAL COEFFICIENTS

For cubic materials there are three independent components of the piezo-optical tensor, P_{11}, P_{12}, and P_{44}.[55] When using RDS one obtains the irreducible components $P_{11}-P_{12}$, corresponding to an applied shear stress of Γ_{12} symmetry (i.e., along [001]), and P_{44}, corresponding to a

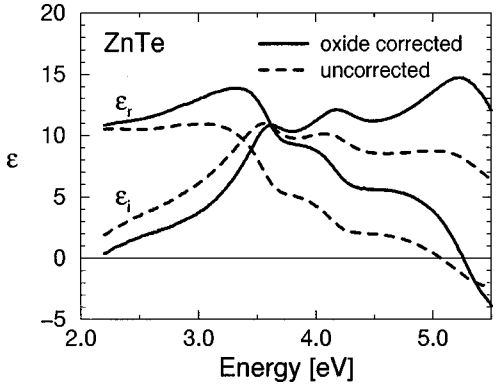

FIG. 3. Real (ε_r) and imaginary (ε_i) parts of the pseudodielectric function of unstressed ZnTe as measured by ellipsometry at room temperature. Data corrected and uncorrected for an oxide overlayer are given.

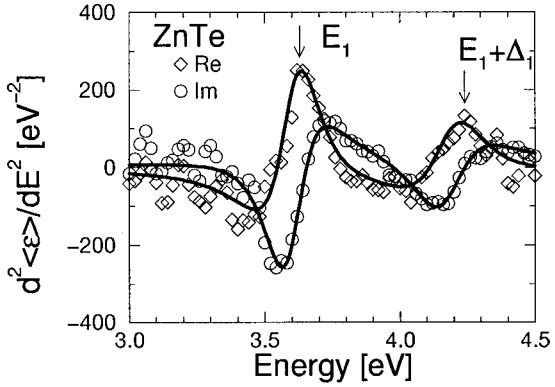

FIG. 4. Second derivative of the pseudodielectric function of ZnTe, as corrected for a surface overlayer, shown in Fig. 3 in the vicinity of the E_1 and $E_1+\Delta_1$ transitions. The solid lines represent fitted values obtained with the excitonic line shapes of Eq. (2). The corresponding fitted parameters are given in Table I.

shear stress of Γ_{15} symmetry (i.e., along [111])[48]

$$P_{11}-P_{12}=\frac{\Delta(\varepsilon^{\parallel}-\varepsilon^{\perp})}{\Delta(X||[001])} \tag{3}$$

and

$$P_{44}=\frac{\Delta(\varepsilon^{\parallel}-\varepsilon^{\perp})}{\Delta(X||[111])}, \tag{4}$$

where $\varepsilon^{\parallel}$ and $\varepsilon^{\perp}$ are the respective components of the dielectric tensor parallel and perpendicular to the stress. $X||[001]$ and $X||[111]$ denote the applied stress, X, being parallel to the [001] and [111] crystal directions, respectively. We use the convention that $X<0$ for a compressive stress. Employing RDS one cannot obtain the piezo-optical coefficient corresponding to hydrostatic stress $P_{11}+2P_{12}$. Therefore, it is not possible to obtain the three independent coefficient, P_{11}, P_{12}, and P_{44}, which can be done when using ellipsometry.[5,6,9,10] When measuring $\varepsilon(\omega)$ by means of ellipsometry, the obtained data are sensitive to the presence of overlayers, see Figs. 1 and 3. RDS is a differential method in which the overlayer effects largely cancel when measuring $\varepsilon^{\parallel}-\varepsilon^{\perp}$; i.e., the overlayer effects are the same for $\varepsilon^{\parallel}$ and $\varepsilon^{\perp}$.[48] The changes in the dielectric function of the oxide overlayer with stress can be neglected since there are no critical points in the experimental range.[6]

Since the piezo-optical coefficients correspond to linear-response functions, their real and imaginary parts are Kramers-Kronig (KK) conjugates. This feature gives a possibility to check the consistency of the data. In order to do so, we calculate[6]

$$\mathrm{Re}[P_{ij}(\omega)]=-\frac{2}{\pi}P\int\frac{\omega'\,\mathrm{Im}[P_{ij}(\omega)]}{\omega'^2-\omega^2}d\omega'+C, \tag{5}$$

where P denotes the principal value of the integral, and C is a constant that was used to fix the overall amplitude (i.e., a background due to transitions other than E_1 and $E_1+\Delta_1$). We did not extrapolate P_{ij} outside the experimental range. The constant C should thus include the effect of P_{ij} outside the experimental range, provided all critical points under consideration lie well within that range.

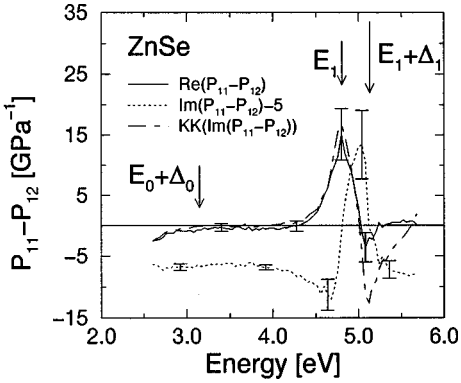

FIG. 5. Real and imaginary parts of the piezo-optical coefficient $P_{11}-P_{12}$ of ZnSe above the fundamental gap. Also shown is the Kramers-Kronig transform of the imaginary part, calculated by using Eq. (5). For clarity, an offset of $-5\ \mathrm{GPa}^{-1}$ was added to the imaginary part. The value for $E_0+\Delta_0$ was taken from Ref. 17.

A. $P_{11}-P_{12}$ and P_{44} of ZnSe

In Fig. 5, the real and imaginary components of the piezo-optical coefficient $P_{11}-P_{12}$ of ZnSe are shown vs photon energy. They have a pronounced structure around the E_1 and $E_1+\Delta_1$ energies. Figure 6 depicts similar data for P_{44} of ZnSe. Also P_{44} has its main structure around E_1 and $E_1+\Delta_1$. The data for $P_{11}-P_{12}$ and P_{44} in the vicinity of the E_1 and $E_1+\Delta_1$ transitions will be analyzed in detail below. With the present technique we cannot detect any structure around the $E_0+\Delta_0$ transitions in $P_{11}-P_{12}$ and P_{44}. The $E_0+\Delta_0$ transition is weak and difficult to detect also in $\varepsilon(\omega)$ measured by ellipsometry.[15] The estimated errors are relatively large since only low stresses could be applied.[48]

The KK conjugates of $P_{11}-P_{12}$ and P_{44}, calculated according to Eq. (5), are shown in Figs. 5 and 6, respectively. For ZnSe, E_1 and $E_1+\Delta_1$ are close to the upper limit of the experimental frequency range. The piezo-optical coefficients are strongly dispersive in this region and the errors due to the finite limits used in Eq. (5) are expected to become relatively large. The line shapes are, however, well reproduced by using Eq. (5), which indicates that they are essentially correct.

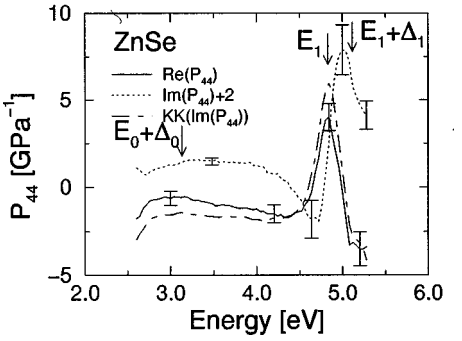

FIG. 6. Real and imaginary parts of the piezo-optical coefficient P_{44} of ZnSe above the fundamental gap, measured at room temperature. Also shown is the Kramers-Kronig transform of the imaginary part, calculated by using Eq. (5). For clarity, an offset of $+2\ \mathrm{GPa}^{-1}$ was added to the imaginary part. The value for $E_0+\Delta_0$ was taken from Ref. 17.

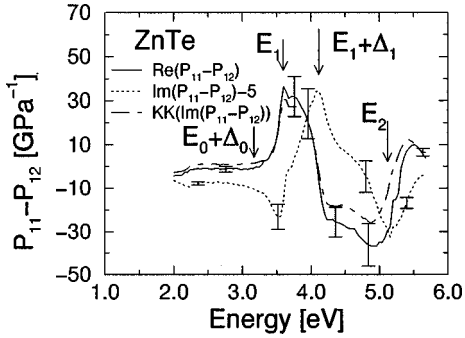

FIG. 7. Real and imaginary parts of the piezo-optical coefficient $P_{11}-P_{12}$ of ZnTe above the fundamental gap, measured at room temperature. Also shown is the Kramers-Kronig transform of the imaginary part, calculated using Eq. (5). For clarity, an offset of $-5\ \mathrm{GPa}^{-1}$ was added to the imaginary part. The values for $E_0+\Delta_0$ and E_2 were taken from Ref. 20.

B. $P_{11}-P_{12}$ and P_{44} of ZnTe

The piezo-optical coefficient $P_{11}-P_{12}$ of ZnTe is shown in Fig. 7 and that of P_{44} in Fig. 8. Both $P_{11}-P_{12}$ and P_{44} have pronounced structures around E_1 and $E_1+\Delta_1$ and also at E_2. The structure of $P_{11}-P_{12}$ and P_{44} around E_1 and $E_1+\Delta_1$ will be analyzed in detail below. As in the case of ZnSe, $E_0+\Delta_0$ cannot be distinguished in the piezo-optical coefficients. In fact, $E_0+\Delta_0$ of ZnTe has just recently been observed in $\varepsilon(\omega)$ measured by ellipsometry.[20] As in the case of ZnSe the estimated errors are large due to the fact that ZnTe is brittle and only low stresses could be applied.

The E_2 structure originates from transitions over a large part of the Brillouin zone. It cannot be modeled by simple analytical expressions, like E_1 and $E_1+\Delta_1$, but requires full band-structure calculations.[5,6,9]

The KK consistency of the real and imaginary parts of $P_{11}-P_{12}$ and P_{44} of ZnTe is good. Since the E_1 and $E_1+\Delta_1$ transitions are not close to the experimental limits, the problems that appeared for ZnSe are not present for ZnTe.

V. DEFORMATION POTENTIALS

The change in gap energies per unit strain is described by deformation potentials. By applying stress along different crystal directions the deformation potentials corresponding

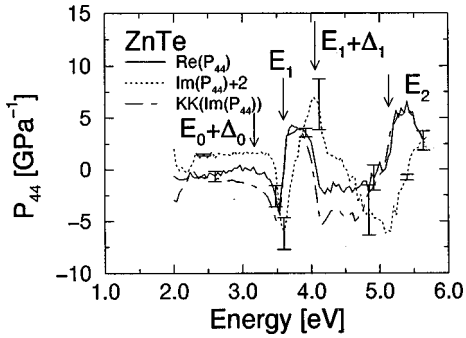

FIG. 8. Real and imaginary part of the piezo-optical coefficient P_{44} of ZnTe above the fundamental gap, measured at room temperature. Also shown is the Kramers-Kronig transform of the imaginary part, calculated with Eq. (5). For clarity, an offset of $+2\ \mathrm{GPa}^{-1}$ was added to the imaginary part.

to different symmetries can be obtained. The piezo-optical coefficients determined in this work are related to the change in electronic structure produced by the applied shear components of the stress. Thus, one can derive expressions, based on a one-electron approximation, that relate the piezo-optical coefficients to the deformation potentials for both the E_0 and the E_1 transitions.[3] For E_0 it has been established that deformation potentials can be determined from the piezo-optical coefficients, by fitting analytical line shapes with the deformation potentials as fitting parameters.[3,21,24,45] For the E_1 and $E_1+\Delta_1$ transitions deformation potentials have in most cases been obtained from the directly measured change in transition energy with applied stress. There are, however, analytical expressions for the relations between the piezo-optical coefficients and the deformation potentials,[3] which can be used to determine the latter.[56] In the case of the brittle ZnSe and ZnTe we were not able to apply the high stresses, which are required when using ellipsometry to determine stress-induced shifts in critical point energies. We therefore determine the deformation potentials of the E_1 and $E_1+\Delta_1$ transitions by fitting analytical line shapes (with parameters obtained from the pseudodielectric function at zero stress) to the experimentally determined $P_{11}-P_{12}$ and P_{44}. For ZnTe we were also able to measure the piezo-optical coefficients around the E_2 and $E_2+\Delta_2$ transitions. These transitions extend over a large part of the Brillouin zone. There are therefore no simple physically meaningful analytical expressions that can be used to represent $\varepsilon(\omega)$ or the piezo-optical coefficients.[5,6,9]

The quantity $P_{11}-P_{12}$, which describes the effects of strains of Γ_{12} symmetry, is related to D_3^3, the deformation potential describing a [001] shear strain (also of Γ_{12} symmetry) by the expression[3]

$$P_{11}-P_{12}=\sqrt{6}D_3^3\left(\frac{\varepsilon^{(E_1)}-\varepsilon^{(E_1+\Delta_1)}}{\Delta_1}\right)(S_{11}-S_{12})+C_{001}. \tag{6}$$

Here, $\varepsilon^{(E_1)}$ and $\varepsilon^{(E_1+\Delta_1)}$ are the contributions of the E_1 and $E_1+\Delta_1$ transitions to $\varepsilon(\omega)$, respectively, Δ_1 the spin-orbit splitting of the corresponding valence-band states and S_{11} and S_{12} are elastic compliance coefficients. The constant C_{001} has been added to account for the contributions from other transitions not resonant around the E_1 and $E_1+\Delta_1$ energies.

P_{44}, which corresponds to strains of Γ_{15} symmetry, can be written as a function of the deformation potentials D_1^5 and D_3^5; the former represents the intervalley effect of a [111] shear strain on the E_1 and $E_1+\Delta_1$ gaps whereas the latter describes the intravalley effect within the valence bands[3]

$$P_{44}=\frac{1}{4\sqrt{3}}\left[-D_1^5\frac{d\varepsilon}{dE_1}+4\sqrt{2}D_3^5\left(\frac{\varepsilon^{(E_1)}-\varepsilon^{(E_1+\Delta_1)}}{\Delta_1}\right)\right]S_{44}+C_{111}. \tag{7}$$

$d\varepsilon/dE_1$ is the derivative of $\varepsilon=\varepsilon^{(E_1)}+\varepsilon^{(E_1+\Delta_1)}$ with respect to the transition energy E_1 and S_{44} an elastic compliance coefficient. Also here a constant, C_{111}, has been added to account for the contribution from other transitions.

As seen in Eqs. (6) and (7), $P_{11}-P_{12}$ and P_{44} both have a contribution proportional to $(\varepsilon^{(E_1)}-\varepsilon^{(E_1+\Delta_1)})/\Delta_1$. These terms arise from stress-induced changes in the matrix elements.[57,56] We denote $(\varepsilon^{(E_1)}-\varepsilon^{(E_1+\Delta_1)})/\Delta_1$ the D_3^3, D_3^5 term. P_{44} has an additional contribution proportional to $d\varepsilon/dE_1$. This term is due to changes in the gap energy with stress.[56,57] We shall call it the D_1^5 term. The analytic expression for the linear combination $P_{11}+2P_{12}$, which describes the effect of a hydrostatic stress, contains only a $d\varepsilon/dE_1$ term since hydrostatic strain does not mix bands of different symmetry.[56] Equations (6) and (7) were derived within an effective-mass approximation. It was assumed that the relevant kinetic energies (and the excitonic binding energies) are small in comparison to the spin-orbit splitting Δ_1. The deformation potentials were assumed to be independent of **k** at the L point and along the Λ direction in the Brillouin zone. The terms $\varepsilon^{(E_1)}$ and $\varepsilon^{(E_1+\Delta_1)}$, represented by Eq. (1), were assumed to be equal except for the energy shift Δ_1. Excitonic effects are, to some extent, taken into account in the line shapes used for $\varepsilon^{(E_1)}$ and $\varepsilon^{(E_1+\Delta_1)}$.

We will now use Eqs. (6) and (7) to determine the deformation potentials D_3^3, D_1^5, and D_3^5. For the terms $\varepsilon^{(E_1)}$, $\varepsilon^{(E_1+\Delta_1)}$ and $d\varepsilon/dE_1$ we use the line shapes in Eq. (1) with the parameters in Table I. Since the hydrostatic piezo-optical coefficient $P_{11}+2P_{12}$ could not be measured, we were not able to determine the hydrostatic deformation potential D_1^1.

A. D_3^3, D_1^5, and D_3^5 of ZnSe

We now use Eq. (1) with the parameters for an excitonic line shape in Table I, to determine the D_3^3, D_3^5 and D_1^5 terms in Eqs. (6) and (7). The obtained line shapes are shown in Fig. 9(a). In order to calculate $P_{11}-P_{12}$ and P_{44} from Eqs. (6) and (7) we used values for the compliance coefficients taken from the literature: $S_{11}=21.1$ TPa^{-1}, $S_{12}=-7.8$ TPa^{-1}, and $S_{44}=24.69$ TPa^{-1}.[58]

The deformation potential D_3^3 was determined by fitting Eq. (6) to $P_{11}-P_{12}$. The fitted curves are shown in Fig. 9(b). Except for D_3^3, the background constant C_{001} was the only fitting parameter; the parameter values obtained from the fit are given in Table II. The value of C_{001} is low in comparison with the amplitude of $P_{11}-P_{12}$. Hence, the contribution to the piezo-optical coefficients from other nonresonant transitions is small.

The line shapes of P_{44} and $P_{11}-P_{12}$ are similar. This line shape is also similar to that of the D_3^3, D_3^5 term displayed in Fig. 9(a). The D_1^5 term has a different line shape that exhibits two peaks (corresponding to E_1 and $E_1+\Delta_1$). For P_{44} the D_3^5 term turns out to be the dominant one. Equation (7) was fitted to the P_{44} spectrum with D_1^5, D_3^5, and C_{111} as parameters. The values of these parameters resulting from the fit are given in Table II and the fitted curves in Fig. 9(c). The contribution from the D_1^5 term can hardly be distinguished in P_{44}, a fact that is reflected in the error bars of the listed value for D_1^5. The contribution from other nonresonant transitions is also small, as indicated by the relatively low value of C_{111}.

The estimated error bars in D_3^3, D_1^5, and D_3^5 were obtained from the values for which the fitted curves are within

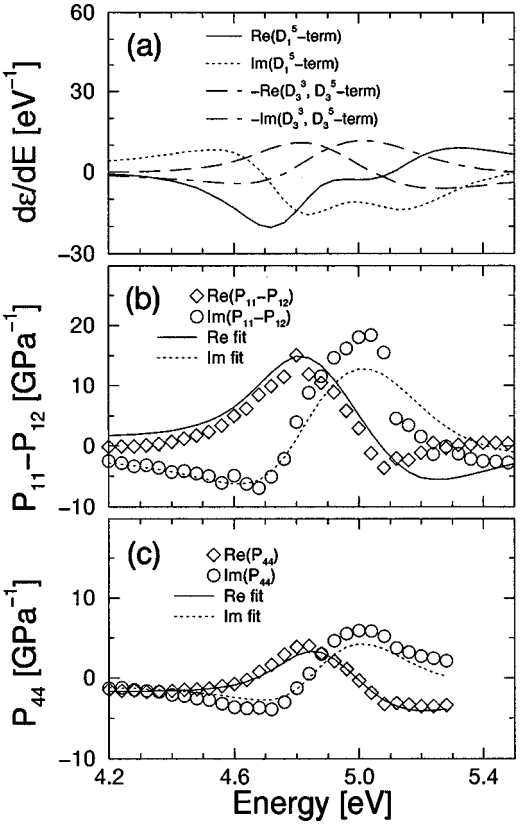

FIG. 9. Fitted line shapes of $P_{11}-P_{12}$ and P_{44} around the E_1 and $E_1+\Delta_1$ critical points of ZnSe. (a) The contribution from the D_3^3, D_3^5, and D_1^5 terms in Eqs. (6) and (7). The minus sign of the D_3^3 and D_3^5 deformation potentials has been included in the D_3^3, D_3^5 term in order to have an easy comparison between curves (a), (b), and (c). (b) Experimental and fitted values for $P_{11}-P_{12}$, and (c) for P_{44}. The fitted curves were obtained with Eqs. (6) and (7), respectively, with the values for the deformation potentials given in Table II. Equation (1) was used to model ε with the parameters given in Table I.

the error bars, which are given with the experimental data in Figs. 5 and 6. These error bars are relatively large since the errors in $P_{11}-P_{12}$ and P_{44} are large. Errors in the line-shape parameters for $\varepsilon^{(E1)}$, $\varepsilon^{(E_1+\Delta_1)}$, and $d\varepsilon/dE_1$ and in the compliances S_{11}, S_{12}, and S_{44} are not included.

We also tried to use the line-shape parameters reported in Ref. 15 for $\varepsilon(\omega)$ around the E_1 and $E_1+\Delta_1$ transitions in Eqs. (6) and (7) but they did not lead to significantly different lineshapes or deformation potentials. Using the parameters obtained for the line shape of a two-dimensional critical point (given in Table I) in Eqs. (6) and (7) the experimental line shapes for $P_{11}-P_{12}$ and P_{44} were not well reproduced; it was not possible to fit Eqs. (6) and (7) to the experimental data. This lends support to the use of an excitonic line shape for the E_1 and $E_1+\Delta_1$ transitions in ZnSe. Equations (6) and (7) contain only differences or derivatives of $\varepsilon(\omega)$ to the first order in energy. Hence, we also determined the line-shape parameters by analyzing the first derivative of $\varepsilon(\omega)$, with respect to photon energy. Using these values the experimental lineshapes were not as well reproduced as in Figs. 9, although the deformation potentials obtained by fitting Eqs. (6) and (7) to the experimental spectra were not significantly different from those in Table II.

B. D_3^3, D_1^5, and D_3^5 of ZnTe

The D_3^3, D_3^5 and D_1^5 terms of ZnTe as calculated from Eq. (1), using the parameters for two-dimensional critical points given in Table I, are displayed in Fig. 10(a). Using D_3^3 and C_{001} as fitting parameters, Eq. (6) was fitted to the experimental spectra of $P_{11}-P_{12}$. The compliances $S_{11}=21.81$ TPa^{-1}, $S_{12}=-10.87$ TPa^{-1} were taken from the literature.[58] The experimental and fitted curves are shown in Fig. 10(b), while the values of the fitted parameters are given in Table II. C_{001} is not negligible in this case, a fact that probably is due to the influence of the E_2 transitions, cf. Fig. 7.

In Fig. 10(c) the spectra of the real and imaginary parts of P_{44} are shown. A comparison with Fig. 10(a) reveals that there is a significant contribution to P_{44} from the D_1^5 term; P_{44} has a line shape different from $P_{11}-P_{12}$, which would not be the case if the D_1^5 term were negligible. This is typical for materials with large spin-orbit splittings.[59] The values of D_1^5, D_3^5, and C_{111} obtained by fitting Eq. (7) to P_{44} (with $S_{44}=32.05$ TPa^{-1})[58] are given in Table II. The error bars in D_3^3, D_1^5, and D_3^5 were estimated in the same way as those for ZnSe and therefore include only the experimental errors in $P_{11}-P_{12}$ and P_{44} (see Figs. 7 and 8), but not any errors in the line-shape parameters or compliances.

The line shapes of $P_{11}-P_{12}$ and P_{44}, calculated with the line-shape parameters for the E_1 and $E_1+\Delta_1$ transition given in Ref. 18 were found to be similar to those in Fig. 10 and the fitted values of the deformation potentials were, within our estimated errors, in agreement with those of Table II. This is also the case if we use the parameters of the excitonic line shape in Table I. Thus, fitting Eqs. (6) and (7) to experimental data for $P_{11}-P_{12}$ and P_{44} does not give any information as to whether the excitonic or the two-dimensional critical point line shapes are to be preferred when dealing with the E_1 and $E_1+\Delta_1$ transitions of ZnTe, a fact which reflects the ''robustness'' of the procedure used to extract the deformation potentials. As in the case of ZnSe, using line-

TABLE II. The deformation potentials D_1^5, D_3^3, and D_3^5 of the E_1 and $E_1+\Delta_1$ transitions in ZnSe and ZnTe. Equations (6) and (7) were used to fit the experimental data of $P_{11}-P_{12}$ and P_{44}. The fitted curves are shown in Figs. 9 and 10, respectively. The dielectric function was modeled with Eq. (1) and the parameters given in Table I. Also given are the complex constant C_{001} and C_{111}, which are the constant backgrounds used in Eqs. (6) and (7), respectively.

	D_1^5 (eV)	D_3^3 (eV)	D_3^5 (eV)	C_{001} (GPa^{-1})	C_{111} (GPa^{-1})
ZnSe	30 ± 30	-17 ± 5	-27 ± 9	$1.7-i1.2$	$-1.6-i0.9$
ZnTe	40 ± 20	-29 ± 8	-15 ± 5	$-8.9+i6.6$	$0.2+i1.1$

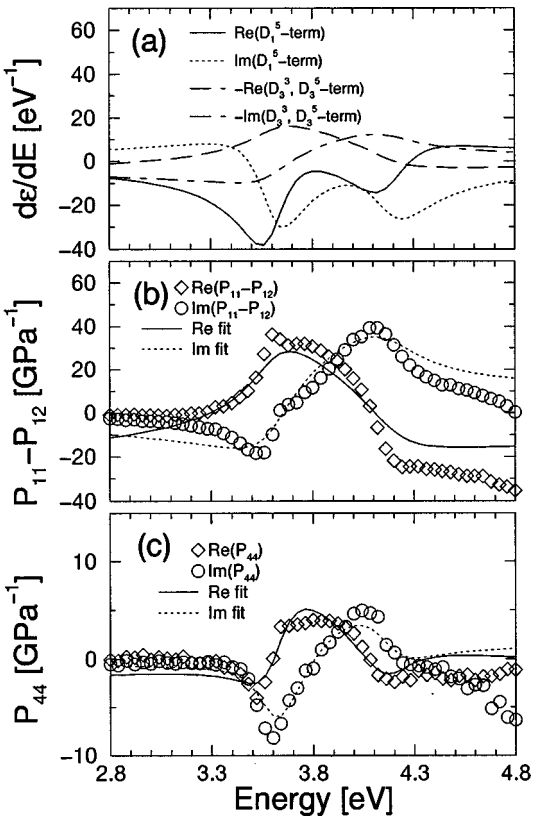

FIG. 10. Fitted line shapes of $P_{11}-P_{12}$ and P_{44} around the E_1 and critical points $E_1+\Delta_1$ of ZnTe. (a) The contribution from the D_3^3, D_3^5, and D_1^5 terms in Eqs. (6) and (7). The minus sign of the D_3^3 and D_3^5 deformation potentials has been included in the D_3^3, D_3^5 term in order to have an easy comparison between curves (a), (b), and (c). (b) Experimental and fitted values for $P_{11}-P_{12}$, and (c) for P_{44}. The fitted curves were obtained with Eqs. (6) and (7), respectively, with the values for the deformation potentials given in Table II. Equation (1) was used to model $\varepsilon(\omega)$ with the parameters given in Table I.

shape parameters obtained by fitting the first derivative of $\varepsilon(\omega)$ with respect to energy did not give different values for the deformation potentials, but lead to a worse line shape of $P_{11}-P_{12}$ and P_{44} calculated with Eqs. (6) and (7), respectively.

VI. DISCUSSION

The deformation potentials of the E_1 and $E_1+\Delta_1$ transitions of ZnSe and ZnTe have been determined by fitting analytical expressions to the measured spectral dependence of the piezo-optical coefficients. For elemental[5,6] and III-V semiconductors[9,10] the change in transition energy with applied stress has allowed a more direct determination of the corresponding deformation potentials. The advantage of this procedure is that the critical point energies of $\varepsilon(\omega)$ can be determined more accurately than the piezo-optical coefficients. The use of Eqs. (6) and (7) for determining D_3^3, D_3^5, and D_1^5 from experimental spectra has to rely heavily on the assumptions made for the line shapes.

It is not obvious what line shape one should use to fit the critical points of $\varepsilon(\omega)$ in the E_1 and $E_1+\Delta_1$ region. We used the standard line shape in Eq. (1), which is only accurate for derivative or differential spectra. This should pose no problem in the present work since in Eqs. (6) and (7) only derivatives and differences of $\varepsilon(\omega)$ occur. As mentioned, we tried also other line shapes for both ZnSe and ZnTe, but the obtained deformation potentials were the same within the estimated errors.

For the E_0 transitions of most semiconductors measured so far the deformation potentials are found to be typically between 1 and 10 eV.[60] The values determined experimentally for the deformation of the E_1 and $E_1+\Delta_1$ transitions in elemental[5,6] and III-V (Refs. 9 and 10) semiconductors are in most cases in this range too. Therefore, the values we find for ZnSe and ZnTe are high in comparison to those found for many other materials. However, II-VI semiconductors are not as well understood as their group IV and II-VI counterparts, in particular the details of their E_1 and $E_1+\Delta_1$ transitions. Furthermore, we had to fit analytical expressions to the piezo-optical coefficients, while for the elemental and III-V semiconductors, stress-induced changes of the transition energies were used. It is worth mentioning that the signs of the deformation potentials in Table II are the same as those found for the corresponding deformation potentials in GaAs (Ref. 9) and InP.[10]

The relatively low values of C_{001} and C_{111} (see Table II) indicate that the contributions from transitions other than E_1 and $E_1+\Delta_1$ are small. This is in contrast to the E_0 transition of both ZnSe (Refs. 21 and 24) and ZnTe,[21,45] which have relatively large constant backgrounds from higher transitions (e.g., the E_1 and $E_1+\Delta_1$ transitions discussed here). The influence from the E_2 transitions on the piezo-optical coefficients at lower energies has sometimes been modeled by a harmonic oscillator[61,62] instead of a constant. With such a model, which involves more parameters, a better fit to experimental data can be achieved. In our case, a slightly better fit to $P_{11}-P_{12}$ and P_{44} of ZnTe at the higher energies in Fig. 10 could be obtained; the values of the determined deformation potentials were, however, not different from those in Table II within the estimated error bars, a fact which again corroborates the ''robustness'' of the deformation potentials obtained here.

In Eqs. (6) and (7), $\varepsilon^{(E_1)}$ and $\varepsilon^{(E_1+\Delta_1)}$ are assumed to be equal except for the energy difference Δ_1. In Figs. 2 and 4 and also in Table I one sees that this is not the case. However, it is not too bad an approximation; the strengths A are the same to within 25% for both ZnSe and ZnTe (for the excitonic and two-dimensional critical point line shapes, respectively, which were used to model the respective piezo-optical coefficients). In InP the strength of the $E_1+\Delta_1$ transition is only $\sim 1/3$ of that of the E_1 counterpart and it was found that Eqs. (6) and (7) could be fitted to experimental data if their strengths were set equal.[10] A similar effect has been seen in the Raman polarizability of Ge.[63]

Equations (6) and (7) implicitly assume that the exciton binding energies are small in comparison with Δ_1. For E_1 and $E_1+\Delta_1$ of ZnSe and ZnTe this assumption may introduce errors. For ZnTe values for the binding energies of the E_1, $E_1+\Delta_1$ exciton of 0.11 eV (Ref. 64) and 0.19 eV (Refs. 18 and 19) have been reported; they are smaller than $\Delta_1=0.58$ eV (Table I), but not by a large factor. For ZnSe it has been estimated that the excitonic binding energies are of the same order as Δ_1.[14,64] If the excitonic binding energies

cannot be neglected in comparison with Δ_1, the excitons of the E_1 and $E_1+\Delta_1$ transitions will mix due to exchange interaction. In this case, the effect of strain on $\varepsilon(\omega)$ should be smaller than if excitons were neglected (see Table V in Ref. 65).

Local-field effects are not included in Eqs. (6) and (7). We do not know what influence they would have on the piezo-optical coefficients, though it is obvious that in a crystal under uniaxial stress, the local fields will be different from those in the unstrained crystal, since the positions of the atoms have changed and the symmetry has been lowered. Local-field effects have been found to introduce anisotropies in the dielectric function of interfaces, in which case the symmetry is changed due to the interface.[66] In ZnSe and ZnTe, which have relatively small infrared dielectric constants, local-field effects are likely to be larger than those in the elemental and III-V semiconductors. We have not found in the literature any theoretical calculations of piezo-optical effects including local-field effects. Calculations of the dielectric function including both excitonic and local-field effects have been made for silicon.[67,68] For the E_1 transition these calculations revealed that local-field and excitonic effects give contributions to $\varepsilon(\omega)$ with opposite signs.[67] Since excitonic effects would give smaller values for the deformation potentials than the one-electron approximation used in Eqs. (6) and (7), local-field effects could be the reason for the possible inadequacy of the one-electron approximation for the calculation of piezo-optical coefficients. Since the analytical expressions used in the determination of the deformation potentials [Eqs. (6) and (7)] are based on the one-electron approximation, the values in Table II should be used with care. It would be of interest to investigate theoretically the effects of local fields and excitons not only on $\varepsilon(\omega)$, but also on the piezo-optical coefficients, particularly since the change in atomic positions and symmetry in a strained crystal should affect the local fields. Furthermore, it would be of interest to investigate theoretically the dependence of these effects on the ionicity of the compound since there are experimental data for elemental, III-V, and II-VI semiconductors. Band-structure calculations of the deformation potentials D_1^5, D_3^3, and D_3^5 are not available for II-VI compounds. They would contribute to clarify the origin of the large values found in the present investigation.

In order to round off this discussion we present in the Appendix a calculation of the strengths $A^{(E_1)}$ and $A^{(E_1+\Delta_1)}$ of a two-dimensional critical point, based on the one-electron band structure. For ZnTe the calculated values are a factor of 2.5 smaller than the ones obtained from the fits to ellipsometric data performed with Eq. (2). For ZnSe, for which the two-dimensional critical point line shape appears to be less accurate, the calculated values are a factor of 3 ($A^{(E_1)}$) and 1 ($A^{(E_1+\Delta_1)}$) times the experimental ones, respectively. A calculation based on a hydrogenic exciton is also presented. It leads to values of $A^{(E_1)}$ and $A^{(E_1+\Delta_1)}$ three times smaller than those fitted for ZnSe. For ZnTe the values calculated for an exciton are six times smaller than the experimental ones. The missing oscillator strength also suggests local-field contributions, which may be more sensitive to strain than the one-electron treatment used here to determine the deformation potentials.

VII. CONCLUSIONS

We have measured the piezo-optical coefficients $P_{11}-P_{12}$ and P_{44} of ZnSe and ZnTe above E_0 using RDS. For ZnSe $P_{11}-P_{12}$ and P_{44} have strong structures around the E_1 and $E_1+\Delta_1$ transitions. This was also found for ZnTe, but in this case we could also see the corresponding effects of the E_2 transition. For ZnSe some problems were encountered with the Kramers-Kronig consistency of the data. They seem to be due to the fact that the E_1 and $E_1+\Delta_1$ transitions are close to the limit of the experimental interval. The spectra of the real and imaginary parts of $P_{11}-P_{12}$ and P_{44} of ZnTe show excellent Kramers-Kronig consistency.

The deformation potentials D_3^5, D_3^3, and D_1^5 were determined by fitting analytical expressions to the experimentally determined spectra of $P_{11}-P_{12}$ and P_{44}. This way of determining deformation potentials of the E_1 and $E_1+\Delta_1$ transitions is not as well established as the corresponding one for the E_0 transition. The values determined for the deformation potentials are high in comparison with those found for elemental and III-V semiconductors, obtained from the measurement of the change in transition energy with applied stress. The reason for these high values may be the large excitonic binding energies, which may lead to a break down of the one-electron approximation, and hence introduce errors in the expressions for $P_{11}-P_{12}$ and P_{44}. Another reason could be that local-field effects cannot be neglected in II-VI semiconductors.

APPENDIX

For a two-dimensional critical point, the strengths of the E_1 and $E_1+\Delta_1$ transitions are, within the one-electron approximation, given by[3]

$$A^{(E_1)}=\frac{16\sqrt{3}}{9}\frac{(E_1+\Delta_1/3)}{a_0E_1^2}, \tag{A1a}$$

$$A^{(E_1+\Delta_1)}=\frac{16\sqrt{3}}{9}\frac{(E_1+2\Delta_1/3)}{a_0(E_1+\Delta_1)^2}, \tag{A1b}$$

where a_0 is the lattice constant.

In the case of excitonic transitions, the strengths are given by[69]

$$A^{(E_1)}=\frac{64\sqrt{3}}{81\pi^4}\frac{a_0^3}{E_1^2\varepsilon_s^3}(E_1+\Delta_1/3)^3, \tag{A2a}$$

$$A^{(E_1+\Delta_1)}=\frac{64\sqrt{3}}{81\pi^4}\frac{a_0^3}{(E_1+\Delta_1)^2\varepsilon_s^3}(E_1+2\Delta_1/3)^3, \tag{A2b}$$

where ε_s is the static dielectric constant.

To calculate the strengths $A^{(E_1)}$ and $A^{(E_1+\Delta_1)}$ by Eqs. (A1) and (A2) we take the values for a_0 ($a_0=5.669$ Å, for ZnSe and $a_0=6.100$ Å for ZnTe)[58] and ε_s ($\varepsilon_s=5.8$ at $\lambda=10$ μm for ZnSe and $\varepsilon_s=7.0$ at $\lambda=10$ μm for ZnTe)[13] from the literature. For E_1 and $E_1+\Delta_1$ we use the values in Table I. In Table I strengths calculated with Eqs. (A1) and (A2) are given.

[1] H. Morkoc, S. Strite, G. B. Gao, M. E. Lin, B. Sverdlov, and M. Burns, J. Appl. Phys. **76**, 1363 (1994).
[2] J. Y. Marzin, J. M. Gérard, P. Voisin, J. A. Brum, in *Semiconductors and Semimetals*, edited by T. P. Pearsall (Academic, New York, 1990), Vol. 32, Chap. 3.
[3] M. Cardona, in *Light Scattering in Solids II*, edited by M. Cardona and G. Güntherodt (Springer-Verlag, Berlin, 1982), p. 19.
[4] M. Cardona, D. Rönnow, and P. V. Santos, Thin Solid Films **313-314**, 10 (1998).
[5] P. Etchegoin, J. Kircher, and M. Cardona, Phys. Rev. B **47**, 10 292 (1993).
[6] P. Etchegoin, J. Kircher, M. Cardona, and C. Grein, Phys. Rev. B **45**, 11 721 (1992).
[7] D. Rönnow, N. E. Christensen, and M. Cardona, preceding paper, Phys. Rev. B **59**, 5575 (1999).
[8] D. E. Aspnes, J. P. Harbison, A. A. Studna, and L. T. Florez, J. Vac. Sci. Technol. A **6**, 1327 (1988).
[9] P. Etchegoin, J. Kircher, M. Cardona, C. Grein, and E. Bustarret, Phys. Rev. B **46**, 15 139 (1992).
[10] D. Rönnow, P. Santos, M. Cardona, E. Anastassakis, and M. Kuball, Phys. Rev. B **57**, 4432 (1998).
[11] N. Suzuki and K. Tada, Jpn. J. Appl. Phys., Part 1 **22**, 441 (1983).
[12] F. Canal, M. Grimsditch, and M. Cardona, Solid State Commun. **29**, 523 (1979).
[13] L. Ward, in *Handbook of Optical Constants of Solids II*, edited by E. Palik (Academic, New York, 1991), p. 737.
[14] S. Adachi and T. Taguchi, Phys. Rev. B **43**, 9569 (1991).
[15] Y.-D. Kim, S. L. Cooper, M. V. Klein, and B. T. Jonker, Appl. Phys. Lett. **62**, 2387 (1993).
[16] R. Dahmani, L. Salamanca-Riba, N. V. Nguyen, D. Chandler-Horowitz, and B. T. Jonker, J. Appl. Phys. **76**, 514 (1994).
[17] C. C. Kim and S. Sivananthan, Phys. Rev. B **53**, 1475 (1996).
[18] S. Adachi and K. Sato, Jpn. J. Appl. Phys., Part 1 **31**, 3907 (1992).
[19] K. Sato and S. Adachi, J. Appl. Phys. **73**, 926 (1993).
[20] Y. D. Kim, S. G. Choi, M. V. Klein, S. D. Yoo, D. E. Aspnes, S. H. Xin, and J. K. Furdyna, Appl. Phys. Lett. **70**, 610 (1997).
[21] P. Y. Yu and M. Cardona, J. Phys. Chem. Solids **34**, 29 (1973).
[22] J. P. Szczesniak, D. Cuddeback, and J. C. Corelli, J. Appl. Phys. **47**, 5356 (1976).
[23] K. K. Dubenski, A. A. Kaplyanskii, and N. G. Lozovskaya, Fiz. Tverd. Tela (Leningrad) **8**, 2068 (1966) [Sov. Phys. Solid State **8**, 1644 (1967)].
[24] K. Tada, K. Kikuchi, and K. Sato, Jpn. J. Appl. Phys. **16**, 757 (1977).
[25] K. Ando, K. Yamabe, S. Hamada, and C. Hamaguchi, J. Phys. Soc. Jpn. **41**, 1593 (1976).
[26] L. F. Goldstein, J. S. Thompson, J. B. Schroeder, and J. E. Slattery, Appl. Opt. **14**, 2432 (1975).
[27] L. K. Andrianova, I. I. Afanasev, A. A. Demidenko, A. A. Dunaev, I. A. Mironov, and G. T. Petrovski, Opt. Mekh. Promst. **57**, 36 (1990) [Sov. J. Opt. Technol. **57**, 615 (1990)].
[28] G. F. Schötz, E. Griebl, H. Stanzl, T. Reisinger, and W. Gebhardt, Mater. Sci. Forum **182-184**, 271 (1995).
[29] E. Griebl, G. F. Schötz, C. Birzer, W. Kerner, T. Reisinger, B. Hahn, and W. Gerhardt, Acta Phys. Pol. A **88**, 995 (1995).
[30] R. L. Gunshor, L. A. Kolodziejski, M. R. Melloch, M. Vaziri, C. Choi, and N. Otsuka, Appl. Phys. Lett. **50**, 200 (1987).
[31] D. Fröhlich, W. Nieswand, U. W. Pohl, and J. Wrzesinski, Phys. Rev. B **52**, 14 652 (1995).
[32] S. Ves, K. Strössner, N. E. Christensen, C. K. Kim, and M. Cardona, Solid State Commun. **56**, 479 (1985).
[33] Y. R. Lee, A. K. Ramdas, L. A. Kolodziejski, and R. L. Gunshor, Phys. Rev. B **38**, 13 143 (1988).
[34] B. Rockwell, H. R. Chandrasekhar, M. Chandrasekhar, A. K. Ramdas, M. Kobayashi, and R. L. Gunshor, Phys. Rev. B **44**, 11 307 (1991).
[35] M. Stoehr, F. Hamdani, J. P. Lascaray, and M. Maurin, Phys. Rev. B **44**, 8912 (1991).
[36] F. Cerdeira, J. S. DeWitt, U. Rössler, and M. Cardona, Phys. Status Solidi **41**, 735 (1970).
[37] N. E. Christensen and I. Gorczyca, Phys. Rev. B **44**, 1707 (1991).
[38] R. A. Casali and N. E. Christensen, Solid State Commun. (to be published).
[39] L. E. Solovev and M. O. Chalka, Fiz. Tverd. Tela (Leningrad) **22**, 970 (1980) [Sov. Phys. Solid State **22**, 568 (1980)].
[40] B. Koopmans, P. V. Santos, and M. Cardona, Phys. Status Solidi B **205**, 419 (1998).
[41] A. Friberg and I. Holwech, Appl. Phys. **11**, 383 (1976).
[42] J. Baillou, Rev. Phys. Appl. **17**, 377 (1982).
[43] N. D. Nedashkovskaya, Opt. Spektrosk. **55**, 966 (1983) [Opt. Spectrosc. (USSR) **55**, 584 (1983)].
[44] V. M. Agranovich and V. L. Ginsburg, *Crystal Optics with Spatial Dispersion and the Theory of Excitons* (Springer-Verlag, Heidelberg, 1984).
[45] S. Adachi and C. Hamaguchi, J. Phys. Soc. Jpn. **43**, 1637 (1977).
[46] M. Yamada, K. Yamamoto, and K. Abe, J. Phys. D **10**, 1309 (1977).
[47] M. Lindner, G. F. Schötz, P. Link, H. P. Wagner, W. Kuhn, and W. G. Gebhardt, J. Phys.: Condens. Matter **4**, 6401 (1992).
[48] D. Rönnow, L. F. Lastras-Martínez, M. Cardona, and P. V. Santos, J. Opt. Soc. Am. A (to be published).
[49] G. Theodorou and G. Tsegas, Phys. Status Solidi B **207**, 541 (1998).
[50] G. Theodorou and G. Tsegas, Phys. Rev. B **56**, 9512 (1997).
[51] Z. H. Levine, H. Zhong, S. Wei, D. C. Allan, and J. W. Wilkins, Phys. Rev. B **45**, 4131 (1992).
[52] D. E. Aspnes, in *Handbook on Semiconductors*, edited by M. Balkanski (North-Holland, Amsterdam, 1980), Vol. 2, Chap. 4A.
[53] R. M. A. Azzam and N. M. Bashara, *Ellipsometry and Polarized Light* (North-Holland, Amsterdam, 1977).
[54] D. E. Aspnes, G. P. Schwartz, G. J. Gualtieri, A. A. Studna, and B. Schwartz, J. Electrochem. Soc. **128**, 590 (1981).
[55] J. F. Nye, *Physical Properties of Crystals* (Oxford University Press, Oxford 1976).
[56] D. D. Sell and E. O. Kane, Phys. Rev. **185**, 1103 (1969).
[57] E. O. Kane, Phys. Rev. **178**, 1368 (1969).
[58] O. Madelung, in *Numerical Data and Functional Relationships in Science and Technology*, edited by O. Madelung, M. Schulz, and H. Weiss, Landolt Börnstein New Series, Group III, Vol. 17, Pt. b (Springer, Heidelberg, 1982).
[59] W. Richter, R. Zeyher, and M. Cardona, Phys. Rev. B **18**, 4312 (1978).
[60] F. H. Pollak, in *Semiconductors and Semimetals* (Ref. 2), Chap. 2.
[61] C. W. Higginbotham, M. Cardona, and F. H. Pollak, Phys. Rev. **184**, 821 (1969).
[62] M. Chandrasekhar, M. H. Grimsditch, and M. Cardona, Phys. Rev. B **18**, 4301 (1978).
[63] M. I. Alonso and M. Cardona, Phys. Rev. B **37**, 10 107 (1988).

[64] Y. Pétroff and M. Balkanski, Phys. Rev. B **3**, 3299 (1971).
[65] H. R. Chandrasekhar, P. Fisher, A. K. Ramdas, and S. Rodriguez, Phys. Rev. B **8**, 3836 (1973).
[66] W. L. Mochan and R. G. Barrera, Phys. Rev. Lett. **55**, 1192 (1985).
[67] W. Hanke and L. J. Sham, Phys. Rev. Lett. **43**, 387 (1979).
[68] S. Albrecht, L. Reining, R. Del Sole, and G. Onida, Phys. Rev. Lett. **80**, 4510 (1998).
[69] P. Lautenschlager, M. Garriga, S. Logothetidis, and M. Cardona, Phys. Rev. B **35**, 9174 (1987).